Korean Journal of Chemical Engineering
https://doi.org/10.1007/s11814-024-00252-9

ORIGINAL ARTICLE

Improvements in Photoluminescence Efficiency and Stability of $CsPbBr_3$ Nanocrystals Through 3-Aminopropyltriethoxysilane Treatment

Seung-Beom Cho[1] · Min-Jae Kim[1] · Il-Kyu Park[1]

Received: 21 July 2024 / Revised: 31 July 2024 / Accepted: 5 August 2024

Abstract
A representative metal halide perovskite, $CsPbX_3$, has received much attention for its high photoluminescence (PL) efficiency and broad emission spectral range covering ultraviolet to infrared. Even with the focused investigations, they still suffer from poor emission stability from surface-induced defects. The inherent instability of perovskites is caused by moisture in the ambient, which leads to a reduction in the luminescence efficiency and deterioration of emission stability. In this study, we report a method to annihilate the surface defects in $CsPbBr_3$ nanocrystals (NCs), which enhances their photoluminescence efficiency by forming a SiO_x shell structure using a 3-aminopropyltriethoxysilane (APTES). The APTES was treated during the synthesis of $CsPbBr_3$ NCs through supersaturation and re-precipitation processes. The optical investigations confirmed that the PL intensity and emission stability of the $CsPbBr_3$ NCs improved with the APTES treatment. The structural investigations using X-ray diffraction and transmission electron microscopy showed that optical analysis was carried out through photoluminescence and laser optical analysis using lasers at 400 nm and 365 nm wavelengths. These findings present an innovative solution to the instability issues of $CsPbBr_3$ and suggest possibilities for its utilization in various application fields. Future research should focus on further understanding the scalability of this method and its practical applicability.

Keywords Perovskite · $CsPbBr_3$ · Nanocrystals · Surface passivation · APTES

Introduction

Hybrid metal halide perovskites have attracted significant attention for next-generative optoelectronic materials due to their unique optical and electrical properties, such as broad emission wavelength ranges by bandgap engineering, high color gamut, sharp and narrow emission peak, and large exciton binding energy [1–7]. In addition, they provide relatively simple fabrication and synthesis processes with vacuum technology and solution processes, enabling low-cost manufacturing processes [7–10]. They exhibit high quantum efficiency and excellent optical properties, making them versatile for various applications, particularly in the display industry. The structure of halide perovskite materials, consisting of the ABX_3 configuration, where the A site accommodates a monovalent cation including Cs and various organics, the B site accommodates a divalent cation, and the X site accommodates a monovalent anion. Especially, cesium lead halide ($CsPbX_3$; X = Cl, Br, and I) materials have been extensively investigated due to their high photoluminescence (PL) and internal quantum efficiency, easy bandgap tuning within the visible spectrum, simple solution processability, and high color purity due to narrow emission spectra [7–10]. However, the intrinsic instability of $CsPbBr_3$ quantum dots (NCs) due to surface defects in humid conditions remains a significant challenge for practical applications [9, 10]. Moisture-induced degradation from surface defects leads to reduced exciton recombination efficiency and deteriorated luminescent properties, along with ligand losses due to the inherent ion properties of perovskites when using polar solvents [11]. Additionally, their low formation energy makes them susceptible to external impacts.

Seung-Beom Cho, Min-Jae Kim have contributed equally to this work.

✉ Il-Kyu Park
pik@seoultech.ac.kr

[1] Department of Materials Science and Engineering, Seoul National University of Science and Technology, Seoul 01811, South Korea

Published online: 12 August 2024

Various methods, such as core–shell structures, ligand exchange, and metal doping, have been reported to enhance the stability and the PL quantum yield (PLQY) of $CsPbBr_3$ NCs to address these issues. The core–shell structure of NCs is a specialized configuration that enhances the optical and electronic properties of the nano-structured semiconductor particles [12–15]. The shell layer passivates the surface of the core NCs, reducing the number of surface defects that can trap charge carriers and quench PL. Especially, the inert shell layer protects the core NCs from oxidation and other environmental degradation. In this way, the shell layer can increase the efficiency of photon emission and improve the emission stability by reducing non-radiative recombination paths. In addition, the surface ligand exchange process is a critical step that modifies the surface chemistry, affecting the stability, solubility, and optoelectronic properties of the semiconductor NCs. Initially, the $CsPbBr_3$ NCs are capped with surface ligands, typically long-chain organic molecules like oleic acid (OA) and oleylamine (OAm). However, the initial ligands may not provide adequate passivation against environmental factors such as moisture, oxygen, and light. The initial ligands are typically non-polar, limiting solubility to non-polar solvents. Meanwhile, the ligand exchange with more polar or functionalized ligands can enable dispersion in a broader range of solvents, facilitating different fabrication processes and integration into various matrices. Therefore, various ligand exchange processes have been investigated using short-chain organic, inorganic, and functional ligands. The short-chain ligands, such as butylamine or octylamine, and inorganic ligands, like other halide ions, could improve solubility in polar solvents and enhance charge transport properties. Functional ligands, such as thiol or carboxylate groups, can also provide specific binding sites or improve compatibility with different substrates or polymers. In this way, ligand exchange is a promising strategy to enhance the emission efficiency and protect the NCs from degradation.

In this study, 3-aminopropyltriethoxysilane (APTES) was post-treated during the synthesis process of $CsPbBr_3$ NC ink using the supersaturation and reprecipitation methods. The APTES treatment on the $CsPbBr_3$ NCs is expected to induce the SiO_2-induced core–shell structures and partial surface ligand exchange. This treatment could improve the stability against moisture and polar solvents and the PL efficiency of the $CsPbBr_3$ NCs. Spin-coating APTES-coated $CsPbBr_3$ NC ink on glass substrates demonstrated enhanced PL stability over time, depending on the amount of the added APTES.

Experimental

Synthesis of Pristine and APTES-Treated $CsPbBr_3$ NCs

The $CsPbBr_3$ NCs were synthesized using the supersaturation and re-precipitation method, as shown in Fig. 1. The surface of $CsPbBr_3$ NCs was treated using the APTES reagent. To prepare the precursor solutions, 0.04 mmol of CsBr (99.9%, metal basis) and 0.04 mmol of $PbBr_2$ (99.998%, metal basis) were dissolved in 1 mL of *N,N*-dimethylformamide (DMF, anhydrous, guaranteed reagent) with 60 µL of OAm (70%, technical grade) in an oversaturated state under stirring. Then, 1 mL of precursor solution was dropped into 20 mL of toluene mixed with OA (10 vol%) under vigorous stirring followed by centrifugations at 12,000 rpm for 5 min. The solution was then filtered to remove impurities and undissolved sources, yielding a clean precursor. To synthesize APTES-treated $CsPbBr_3$ NC solutions, toluene (special grade) solution with OA and APTES were mixed

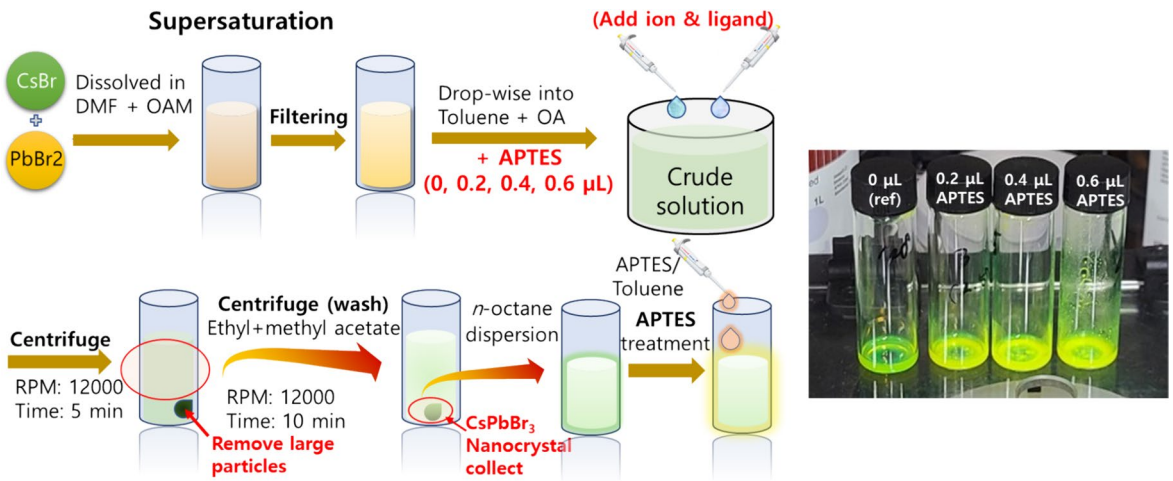

Fig. 1 Schematic synthesis process illustrating the preparation of $CsPbBr_3$ NCs and post-treatment of APTES. The figures are the emission images of the $CsPbBr_3$ NC solutions showing bright emissions even under room light conditions

and stirred at room temperature. The toluene solutions containing OA with various amounts of APTES (0, 0.2, 0.4, and 0.6 µL) were injected drop-wise into the precursor solutions. The mixed solutions were stirred for 20 s, which resulted in the APTES-treated $CsPbBr_3$ NCs. The solutions were centrifuged at 12,000 rpm for 5 min to remove the larger precipitated particles and residues. Methylacetate and ethylacetate were added to the remaining solution at the same volume ratio, followed by centrifugation at 12,000 rpm for 10 min to remove the remaining impurities. The precipitated APTES-treated $CsPbBr_3$ NCs were dispersed in the *n*-octylamine. The APTES-treated $CsPbBr_3$ NC solutions showed bright green emission, as shown in Fig. 1. The pristine and APTES-treated $CsPbBr_3$ NC ink solutions were spin-coated onto the glass substrates to fabricate thin films. Spin coating was carried out at 2000 rpm for 45 s.

Characterizations and Instruments

The optical characterization of $CsPbBr_3$ NCs was performed using a UV–visible spectrophotometer (Agilent 8453). The emission characterizations by PL spectra and emission images were measured using 405 nm laser and UV lamp with wavelength at 365 nm. The emission intensity was monitored using a spectrophotometer (MAYA 2000 PRO). The compositional crystal constructions of the $CsPbBr_3$ NCs were analyzed using X-ray diffraction (XRD, Bruker D8 Advance) by measuring a Cu $K\alpha$ radiation source with $\lambda = 0.154$ nm at a 2θ range of 10°–50°. The microscopic and morphology identifications of the $CsPbBr_3$ NCs were observed in a high-resolution (HR-TEM; JEM-2100F).

Results and Discussion

Structural Properties of the APTES-Treated $CsPbBr_3$ NCs

Figure 2 shows the TEM images of the pristine and APTES-treated $CsPbBr_3$ NCs. As shown in Fig. 2a, d, the pristine $CsPbBr_3$ NCs show cuboidal shape morphologies due to the cubic structure. The average particle size is about 6.3 nm. The $CsPbBr_3$ NCs showed well-defined crystal structures of uniform facets in the high-resolution-TEM (HR-TEM) images, indicating high crystalline quality. The APTES-treated $CsPbBr_3$ NCs showed a similar particle shape and size distribution to the pristine one. Notably, there is no significant change in the cuboidal morphology of $CsPbBr_3$ NCs, and their lattice fringes were maintained with well defined even with increased APTES-treatment contents (Fig. 2(b) ~ (f)). The size of $CsPbBr_3$ NCs increased slightly to over 7.2 nm, increasing the APTES content to 0.6 µL, as shown in Fig. 2(c) and (f). Therefore, although the crystallinity and shape of $CsPbBr_3$ NCs are maintained despite the changes in the APTES content, their size increases slightly. This indicates that the APTES additive does not influence the crystallinity of $CsPbBr_3$ NCs while affecting the size.

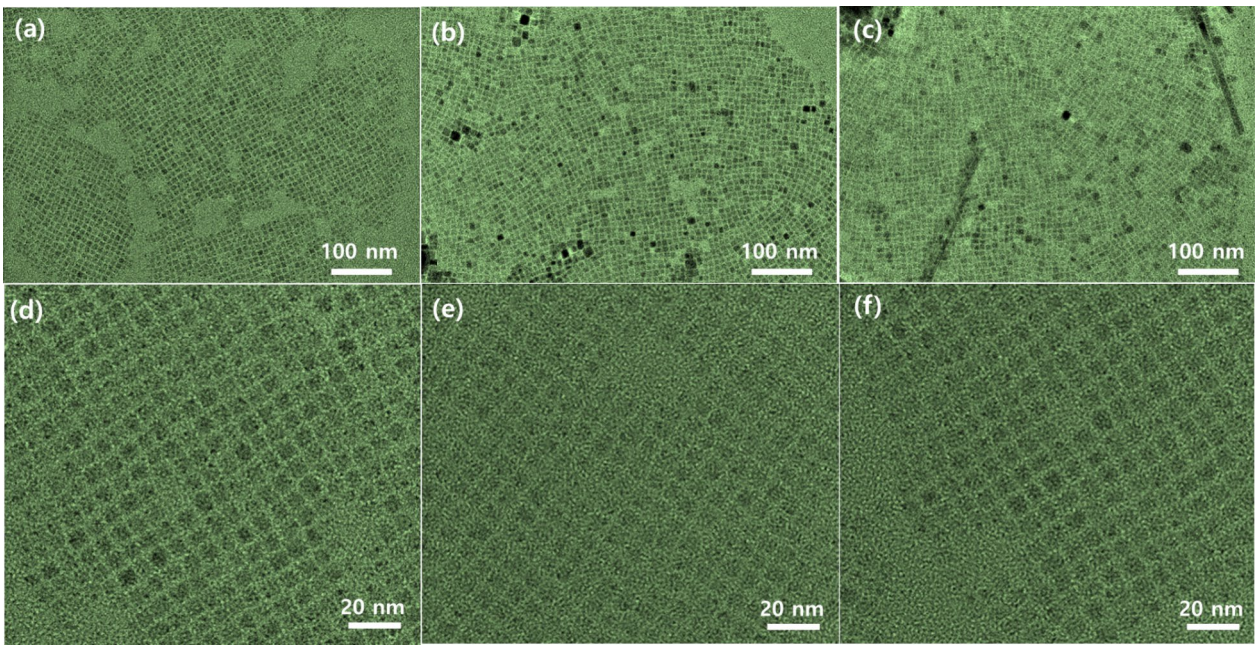

Fig. 2 TEM images of synthesized $CsPbBr_3$ NCs: **a** pristine $CsPbBr_3$ NCs; **b** 0.2 µL of APTES-treated NCs; **c** 0.6 µL of APTES-treated NCs. HR-TEM images of synthesized $CsPbBr_3$ NCs: **d** pristine $CsPbBr_3$ NCs; **e** 0.2 µL of APTES-treated NCs; **f** 0.6 µL of APTES-treated NCs

This would be due to the rearrangement of atoms between the $CsPbBr_3$ NCs during the APTES-post-treatment process. During the APTES treatment, the ligands inevitably detach and reattach from the surface of $CsPbBr_3$ NCs. The other reason would be forming a very thin shell layer on the $CsPbBr_3$ NC surface by APTES treatment.

The structural evolution of the APTES-treated $CsPbBr_3$ NCs was investigated by XRD, as shown in Fig. 3. The $CsPbBr_3$ NCs exhibited the typical cubic phase (JCPDS No. 18–0346) with perovskite structure [7–10]. The APTES-treated $CsPbBr_3$ NCs showed the same diffraction patterns despite their content with the pristine one. The XRD results showed no trace of a secondary phase like $CsPb_2Br_5$. This indicates that the $CsPbBr_3$ NCs maintained a cubic structure after the APTES treatment. This is similar to the TEM results. Even as the APTES content was increased from 0 to 0.6 µL, no additional diffraction peak was found in the XRD patterns. This indicates an absence of any secondary phase or alloys corresponding to the APTES-related phases like SiO_x. Because of the small amount of added APTES content, the surface of $CsPbBr_3$ NCs is treated by thin SiO_x and APTES-induced ligands rather than by forming bulk SiO_x. Notably, the diffraction peaks gradually shifted to a higher angle side as the APTES content increased from 0 to 0.6 µL. Figure 3(b) shows the variation of the (200) peak position according to the APTES-treatment content. Considering Bragg's law, this peak shift indicates the shrinkage of the $CsPbBr_3$ lattice after the APTES treatment. The APTES treatment can induce the formation of a very thin SiO_x layer on the $CsPbBr_3$ NC surface. During this process, the relaxed $CsPbBr_3$ lattice would be under compressive stress [16]. This results in slight lattice shrinkage after APTES treatment.

Optical Properties of the APTES-Treated $CsPbBr_3$ NCs

Figure 4 shows the optical properties of the $CsPbBr_3$ NCs by the post-treatment of APTES. The effect of APTES treatment on the optical properties of the $CsPbBr_3$ NCs was investigated using UV–visible absorption spectroscopy, as shown in Fig. 4a. With the addition of an APTES precursor, the green emission from the $CsPbBr_3$ NCs became more intense under 365 nm UV lamp illumination while maintaining the emission color consistently, as shown in Fig. 1. The UV–visible absorption spectra showed no significant change in the shape of spectra and position of absorption edges despite a change in the APTES content. The UV–visible absorption spectra of the APTES-treated $CsPbBr_3$ NCs showed a similar shape with a sharp exciton absorption peak at around 500 nm and a steep increase in absorbance. Notably, the NCs showed the absorption peak corresponding to the exciton state despite the variation of the APTES content, which is attributed to the uniform size distribution. The TEM investigations confirmed the uniform size distribution of the pristine and APTES-treated $CsPbBr_3$ NCs.

The pristine $CsPbBr_3$ NCs showed a strong photoluminescence (PL) emission peak at 513 nm with a full width at half-maximum (FWHM) of 98 meV. The FWHM of the APTES-treated $CsPbBr_3$ NCs is between 98 and 103 meV. The PL emission peak is slightly blue-shifted compared to the bulk band gap energy of $CsPbBr_3$ (2.42 eV) [9]. This would be attributed to the weak quantum confinement effect of $CsPbBr_3$ NCs. The average size of the $CsPbBr_3$ NCs is very close to the exciton Bohr radius of $CsPbBr_3$ (7 nm), which can profit from the quantum confinement effect. The quantum confinement effect can describe the size-dependent electronic transitions in the semiconductor NCs or quantum dots. Based on an effective

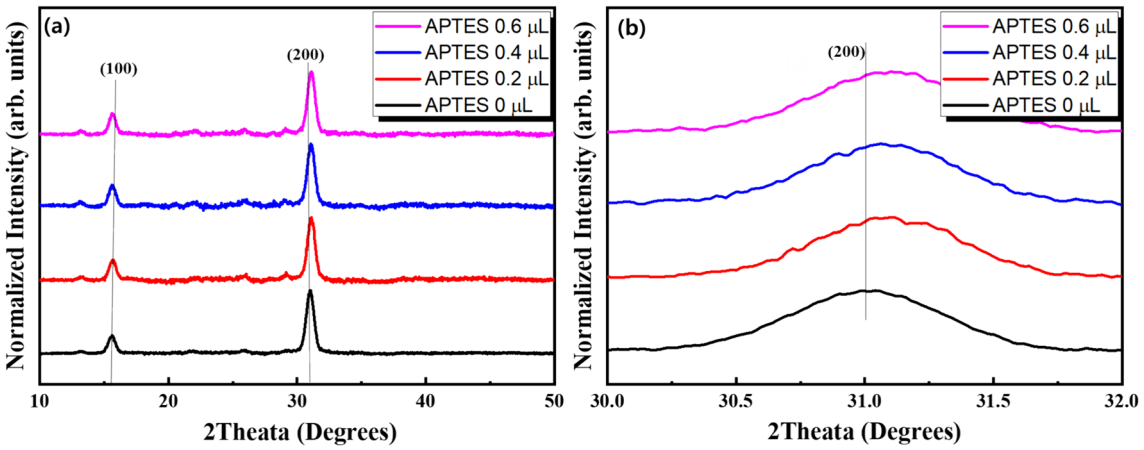

Fig. 3 **a** Normalized XRD patterns of the $CsPbBr_3$ NCs with the variation of APTES content. **b** Variation of (200) peak of the $CsPbBr_3$ NCs with the variation of APTES content

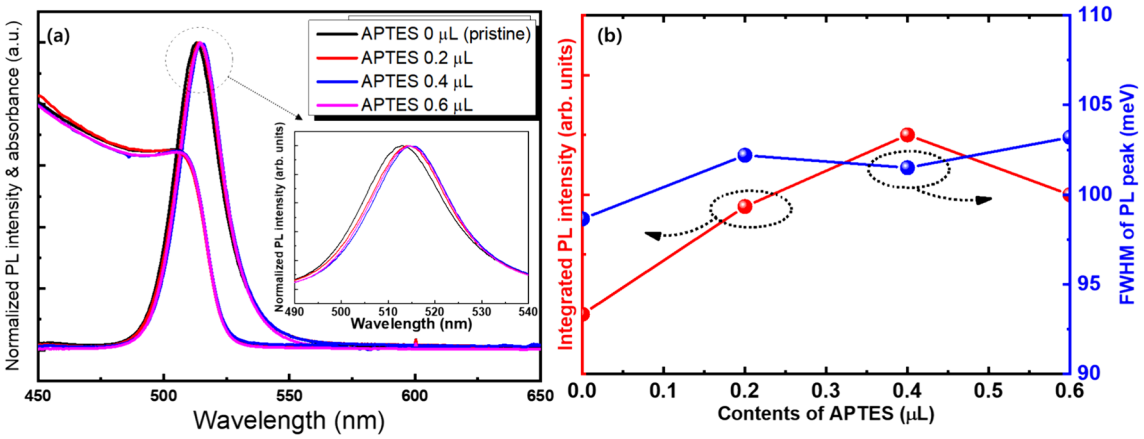

Fig. 4 **a** PL and UV–Vis absorption spectra of $CsPbBr_3$ NC solutions with the variation of APTES additive content. The PL was taken under excitation by a 405 nm laser. **b** Variations of the integrated PL intensity and emission peak width of the $CsPbBr_3$ NC films with the variation of APTES content

mass approximation with a Coulomb interaction, the band gap energy of the NCs can be estimated as follows [17]:

$$E_{NC} = E_g + \frac{h^2}{8r^2}\left(\frac{1}{m_e^*} + \frac{1}{m_h^*}\right) - \frac{1.8e^2}{4\pi\varepsilon_r\varepsilon_0 r},$$

where E_{NC} and E_g are the lowest excitation energy of the NCs and the band gap of bulk structure, respectively. In addition, h is Planck's constant, r is the radius of the NCs, m^*_e is the electron effective mass, m^*_h is the hole effective mass, e is the electron unit charge, ε_r is the relative permittivity of the semiconductors, and ε_0 is the vacuum permittivity. The exciton Bohr radius of the $CsPbBr_3$ is 7 nm. A strong quantum confinement effect occurs for $CsPbBr_3$ NCs with a diameter of less than 7 nm. This size range is close to the mean diameter of the $CsPbBr_3$ NCs synthesized in this study. This NC size range is in the weak quantum confinement region. Therefore, the variation of the emission wavelength is clearly due to the quantum confinement effect in the $CsPbBr_3$ NCs. As the APTES content increases, the emission peaks show red-shift due to the quantum confinement effect. As shown in the TEM results, the size of APTES-treated $CsPbBr_3$ NCs increased compared to the pristine one. Notably, the PL intensity increased with increasing the APTES content, as shown in Fig. 4b. As described above, the APTES treatment forms a very thin SiO_x layer on the $CsPbBr_3$ NC surface, and the amine groups of APTES bind to the surface of the NCs. The thin SiO_x layer acts as a shell layer on the $CsPbBr_3$ NC surface to prevent surface defect-induced non-radiative recombination.

Emission Stability of the APTES-Treated $CsPbBr_3$ NC Thin Films

To investigate the emission stability of the APTES-treated $CsPbBr_3$ NCs, thin films were fabricated by spin coating the solution on a glass substrate, as shown in Fig. 5. Using the NC thin films, the luminescent characteristics and stability over time were compared based on the varying amounts of added APTES. Figure 5 also shows the emission images of the $CsPbBr_3$ NC thin films with variations in the APTES content. With the addition of APTES, the emission from the $CsPbBr_3$ NCs became brighter under illumination by a UV lamp with the same green emission color, as shown in Fig. 5. The micro-PL images under excitations by 405 and 365 nm were compared to investigate the formation of secondary phases. All the samples showed the same emission images regardless of the differences in excitation wavelength. This indicates no secondary phase is formed during the $CsPbBr_3$ NC thin film formation process. The initial luminescent characteristics of $CsPbBr_3$ NCs are maintained despite the APTES-treatment process. The emission stability of the $CsPbBr_3$ NCs was investigated by measuring the PL spectra for the NC thin films after exposure to air ambient for one, two, and three weeks. Figure 6(a)-(c) shows the PL spectra measured after one, two, and three weeks later, respectively. All the $CsPbBr_3$ NCs show degradation of PL intensity with increasing the aging time in air ambient. The degradation of PL efficiency of metal halide perovskites has been well

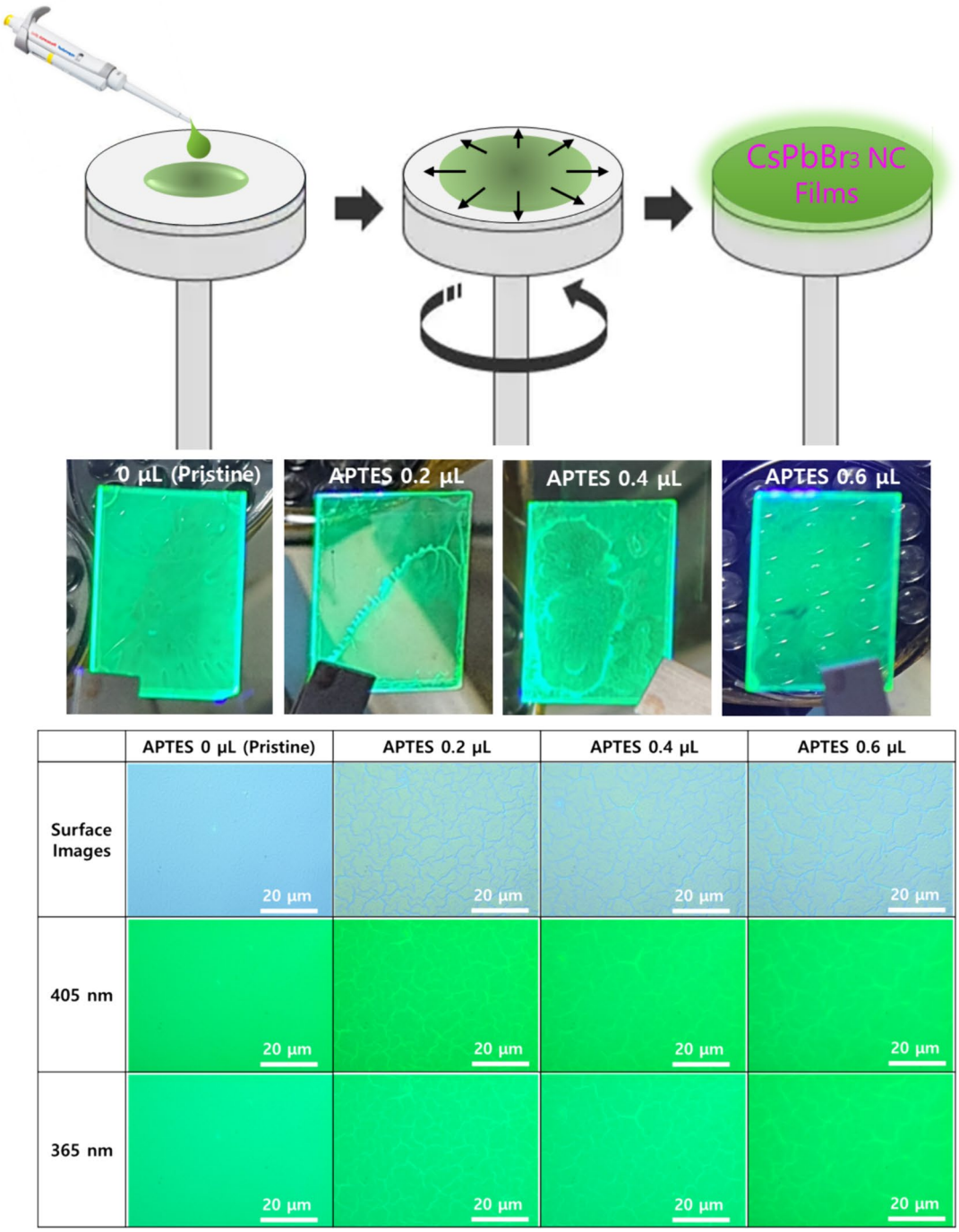

Fig. 5 Schematic synthesis process illustrating the preparation-based spin-coating process. The figures show the emission images of the $CsPbBr_3$ NC films under excitation by the UV lamp. Optical microscope images and microscopic PL emission images of APTES-treated $CsPbBr_3$ NC thin film surfaces with various molar contents of APTES under 405 and 365 nm wavelengths

known. The emission efficiency of perovskite nanostructures mainly degrades due to oxidation and surface defect formation [18, 19]. The metal cations in the perovskite crystal structure are easily oxidized in ambient air as oxygen molecules capture the electrons. Especially in a humid environment, the perovskites are very weak due to their ionic bonding properties [20]. By exposure to moisture, the surface atoms on the $CsPbBr_3$ NCs fall off to generate surface defects. These ultimately degrade the emission efficiency and luminous performances. Therefore, the

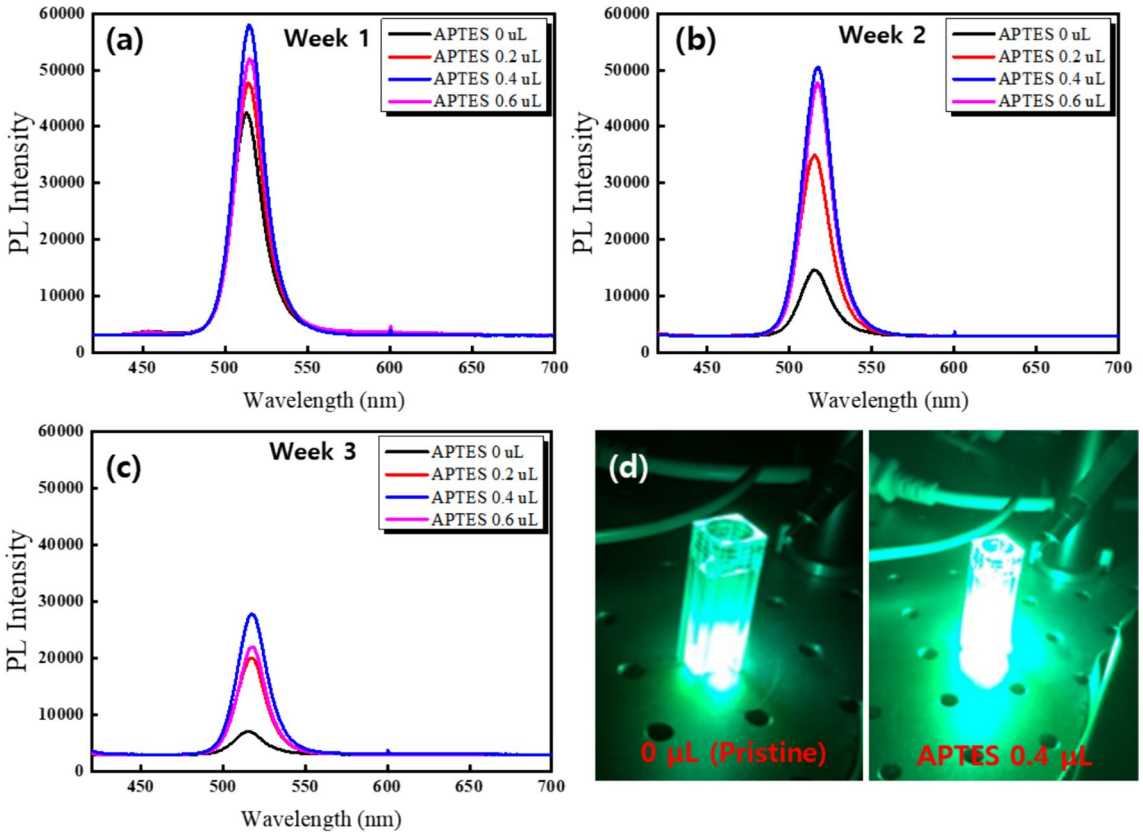

Fig. 6 PL spectra of the SPTES-treated $CsPbBr_3$ NC films after exposure in the air: **a** after 1 week, **b** after two weeks, and **c** after 3 weeks. **d** Emission images of the NC solutions were taken under excitation by a commercial UV lamp. **b** PL spectra and emission images after 3 weeks. The PL was taken under excitation by a 405 nm laser

pristine $CsPbBr_3$ NCs film showed a drastic reduction in PL intensity after 2 and 3 weeks, as shown in Fig. 6(b) and (c). To circumvent these problems, modifying the surface of perovskite NCs or annihilating the surface defects with additional amine-group-based surface ligands is very important. These approaches are effective in improving the stability of oxygen and moisture ambient. In this study, the APTES treatment can form the thin SiO_x shell layers on the $CsPbBr_3$ NCs and provide additional surface ligands. These play a role in passivating anion vacancy sites and removing surface defects. Therefore, the APTES-treated $CsPbBr_3$ NC films showed less reduction in PL intensity even after three weeks compared to the pristine one. In the solution state, the APTES-treated $CsPbBr_3$ NCs maintained emission stability after 3 weeks, as shown in Fig. 6d. In this way, the APTES treatment played a critical role in improving the emission stability and efficiency by eliminating the surface defects and preventing exposure to the ambient. These findings indicate that the amine groups of APTES bind to the surface of the $CsPbBr_3$ NCs, enhancing stability by forming a SiO_x core–shell on the $CsPbBr_3$ surface. This effect mitigates the degradation of stability observed in conventional perovskite-based light-emitting device applications due to atmospheric moisture and polar solvents, and the increased APTES concentration demonstrates a more significant effect.

Conclusions

In this study, we report the enhancement of emission efficiency and stability of $CsPbBr_3$ NCs based on APTES post-treatment. The monodisperse $CsPbBr_3$ NCs with an average size of 6.3 nm were synthesized using the supersaturation and reprecipitation method. The APTES treatment did not affect the crystallinity or shapes of the $CsPbBr_3$ NCs even when the content was increased. Although there were no significant modifications in the structural properties of the $CsPbBr_3$ NCs, their PL intensity and emission stability were improved by increasing the APTES treatment. The investigations showed that the amine groups of APTES bind to the NC surface as an additional surface ligand and form a thin SiO_x shell layer on the $CsPbBr_3$ surface. These effects mitigate the degradation of stability observed in conventional perovskite-based light-emitting device applications due to

atmospheric moisture and polar solvents, and the increased APTES concentration demonstrates a more significant effect.

Acknowledgements This study was supported by the Research program funded by the Seoultech (Seoul National University of Science & Technology).

Author Contributions S.-B. Cho: writing—original draft, conceptualization, writing—review, and methodology. M.-J. Kim: data curation, resources, investigation, formal analysis, writing—review, and methodology, I.-K. Park: supervision, resources, project administration, editing, and funding acquisition.

Data availability The data that support the findings of this study are available from the corresponding author upon reasonable request.

Declarations

Conflict of interest The authors declare that they have no known competing financial interests or personal relationships that could have appeared to influence the work reported in this paper.

References

1. Z.C. Shen, Q.F. Han, X.H. Luo, Y.Z. Shen, Y.B. Wang, Y.B. Yuan, Y.Q. Zhang, Y. Yang, L.Y. Han, Nat. Photonics **18**, 450 (2024)
2. Y. Sun, L. Ge, L. Dai, C. Cho, J. Orri, K. Ji, S. Zelewski, Y. Liu, A. Mirabelli, Y. Zhang, J.-Y. Huang, Y. Wang, K. Gong, M. Lai, L. Zhang, D. Yang, J. Lin, E. Tennyson, C. Ducati, S. Stranks, L.-S. Cui, N. Greenham, Nature **615**, 830 (2023)
3. B.R. Sutherland, E.H. Sargent, Nat. Photon. **10**, 295 (2016)
4. M. Ahmadi, T. Wu, B. Hu, Adv. Mater. **29**, 1605242 (2017)
5. N. Nam, N.T.N. Truong, T. Le, M.R. Pallavoulu, H.J. Jeon, C. Park, Korean J. Chem. Eng. **38**, 187 (2021)
6. C.X. Li, S.B. Cho, D.H. Kim, I.K. Park, Chem. Mater. **34**, 6921 (2022)
7. S.B. Cho, J.W. Jung, Y.S. Kim, C.H. Cho, I.K. Park, CrystEngComm **23**, 2746 (2021)
8. S.B. Cho, J.I. Sohn, S.S. Lee, S.G. Moon, B. Hou, I.K. Park, J. Mater. Chem. C **9**, 7027 (2021)
9. J.B. Cho, S.B. Cho, I.K. Park, J. All. Compd. **891**, 161996 (2022)
10. S.G. Moon, S.B. Cho, K.K. Kim, I.K. Park, J. All. Compd. **858**, 157643 (2021)
11. H.Y. Kim, S.B. Cho, B. Hou, I.K. Park, J. Korean Phys. Soc. **81**, 150 (2022)
12. C.K. Trinh, H. Lee, M.G. So, C.L. Lee, A.C.S. Appl, Mater. Interfaces **13**, 29798 (2021)
13. T.H. Le, Y.N. Ahn, S.J. Park, Korean J. Chem. Eng. **39**, 1065 (2022)
14. J. Iskandar, C.C. Lee, A. Kurniawan, H.M. Cheng, S.W. Liu, S. Biring, Cell Rep. Phys. Sci. **3**, 101170 (2022)
15. W. Lee, G. Park, D. Schröder, Y. Kwon, Korean J. Chem. Eng. **39**, 1624 (2022)
16. A.E. Raevskaya, Y.V. Panasiuk, O.L. Stroyuk, S.Y. Kuchmiy, V.M. Dzhagan, A.G. Milekhin, N.A. Yeryukov, L.A. Sveshnikova, E.E. Rodyakina, V.F. Plyusninde, D.R.T. Zahn, RSC Adv. **4**, 63393 (2014)
17. Y. Kayanuma, Phys. Rev. B **38**, 9797 (1988)
18. N. Aristidou, I. Sanchez-Molina, T. Chotchuangchutchaval, M. Brown, L. Martinez, T. Rath, S.A. Haque, Angew. Chem. Int. Ed. **54**, 8208 (2015)
19. M. Lorenzon, L. Sortino, Q. Akkerman, S. Accornero, J. Pedrini, M. Prato, V. Pinchetti, F. Meinardi, L. Manna, S. Brovelli, Nano Lett. **17**, 3844 (2017)
20. G.E. Eperon, S.N. Habisreutinger, T. Leijtens, B.J. Bruijnaers, J.J. van Franeker, D.W. DeQuilettes, S. Pathak, R.J. Sutton, G. Grancini, D.S. Ginger, ACS Nano **9**, 9380 (2015)